Ferromagnetic resonance in thin films studied via cross-validation of numerical solutions of the Smit-Beljers equation: Application to (Ga,Mn)As

P. Tomczak*
Quantum Physics Division and Faculty of Physics, Adam Mickiewicz University ul. Umultowska 85, 61-614 Poznań, Poland

H. Puszkarski
Surface Physics Division and Faculty of Physics, Adam Mickiewicz University ul. Umultowska 85, 61-614 Poznań, Poland

(Received 9 March 2018; revised manuscript received 22 May 2018; published 10 October 2018)

The method of numerical analysis of experimental ferromagnetic resonance (FMR) spectra in thin films is developed and applied to (Ga,Mn)As thin films. Specifically, it starts with the finding of numerical solutions of Smit-Beljers (SB) equation and continues with their subsequent statistical analysis within the cross-validation (CV) approach taken from machine learning techniques. As a result of this treatment, we are able to reinterpret the available FMR experimental results in diluted ferromagnetic semiconductor (Ga,Mn)As thin films with the resulting determination of magnetocrystalline anisotropy constants. The outcome of CV analysis points out that it is necessary to take into account terms describing the bulk cubic anisotropy up to the fourth order to reproduce FMR experimental results for (Ga,Mn)As correctly. This finding contradicts the widespread conviction in the literature that only the first-order cubic anisotropy term is important in this material. We also provide numerical values of these higher order cubic anisotropy constants for (Ga,Mn)As thin films resulting from the SB-CV approach.

DOI: 10.1103/PhysRevB.98.144415

I. INTRODUCTION: THE EXPERIMENTAL DATA

Gallium manganese arsenide, (Ga,Mn)As, is probably one of the most thoroughly studied diluted ferromagnetic semiconductors. The simultaneous presence of magnetism and conductivity in this material makes it possible to control both the charge and the spin degrees of freedom of the charge carriers. This creates potential spintronic applications. Another reason for the intense research on (Ga,Mn)As is its remarkable magnetic properties, between which magnetic anisotropy plays an important role. It determines, among others, the orientation of magnetization in the absence of an applied magnetic field [1]. Although its understanding is important for prospective applications such as, e.g., memory devices, its origins are far from being fully explained. Magnetocrystalline anisotropy in (Ga,Mn)As, usually described by the single-domain model [2,3], is being investigated by various experimental techniques, such as ferromagnetic resonance (FMR) and spin-wave resonance (SWR) [4]. Most of these methods have been used to obtain information on anisotropy bulk properties of this material. Recently, we have proposed [5] that one can use the SWR to get information on such magnetic properties as surface anisotropy and surface pinning energy of (Ga,Mn)As thin films and their dependence on the orientation of magnetization in the material.

The FMR spectroscopy has long been a good tool for examining magnetocrystalline anisotropy, see, e.g., a recent review on FMR in (Ga,Mn)As thin films [4]. In FMR experiment, since the equilibrium position of the total magnetic moment $\mathbf{M}$ of the sample does not coincide with the direction of the magnetic field, $\mathbf{H}$, due to the presence of magnetocrystalline anisotropy, $\mathbf{M}$ precesses around its equilibrium position with a specific (microwave) frequency ω. By changing the magnetic field $\mathbf{H}$, one hits a resonance field $\mathbf{H}_r$: the precession frequency of $\mathbf{M}$ is equal to the frequency of the spectrometer. The value of the resonance field $\mathbf{H}_r$ strongly depends on its orientation with respect to the examined sample, which is determined by angles θ_H and ϕ_H, see Fig. 1, due to magnetocrystalline anisotropy.

This article presents the results of the analysis of bulk magnetocrystalline anisotropy in (Ga,Mn)As based on examination of the uniform mode in SWR resonance in (Ga,Mn)As thin film [6]. The motivation to carry out this analysis was twofold: First—on the basis of examination of surface mode in the same SWR experiment [6], we have shown [5] that magnetocrystalline *surface* anisotropy in (Ga,Mn)As thin films contains cubic terms up to third order, which is not commonly found among ferromagnets. We wonder if this is also true for *bulk* magnetocrystalline anisotropy. Second,- it was originally shown [6] that to reproduce the experimental dependence of the resonance field on the orientation of the magnetic field with respect to the sample, only the first-order term of cubic anisotropy should be taken into account, which, to some extent, is contradictory to the analysis carried out for the surface [5]. In the meantime, numerical tools have been developed that allow a thorough analysis of this problem. That is why we have considered the old problem again.

At the beginning, let us recall the angular dependencies of resonance field for the uniform mode in ferromagnetic (Ga,Mn)As thin film [6]. They are shown in Ref. [6] in Fig. 5 for the out-of-plane geometry and in Fig. 6 for the in-plane

*Corresponding author: ptomczak@amu.edu.pl

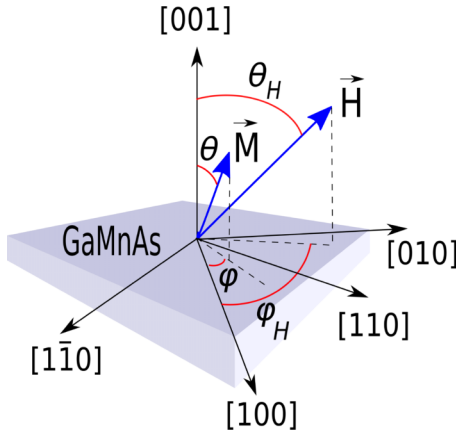

FIG. 1. The coordinate system in which an orientation of the applied magnetic field **H** is described with respect to the sample in the FMR experiment. The field direction is characterized by angles ϑ_H and φ_H measured relative to the sample [001] and [100] axes. The equilibrium direction of the sample magnetization **M** is represented by angles ϑ and φ.

geometry, respectively. We show them again in Fig. 2 to clearly emphasize the difference between the resonance field resulting from the uniaxial anisotropy (plane H_r-ϑ_H) and that resulting from the cubic anisotropy (plane H_r-φ_H). We focus on the interpretation of this experiment because the authors very carefully identified resonance from uniform SWR modes and distinguished it from that for surface modes.

II. PHENOMENOLOGICAL FREE ENERGY

The starting point for the interpretation of experimental data of FMR in (Ga,Mn)As is the phenomenological formula for the free energy of the investigated sample. We assume that there exists a single homogeneous magnetic domain within the sample and that the free energy of a unit volume of the sample consists of Zeeman term F_Z, demagnetization term F_D, and magnetocrystalline anisotropy terms (cubic F_C and uniaxial F_U):

$$F = F_Z + F_D + F_C + F_U. \tag{1}$$

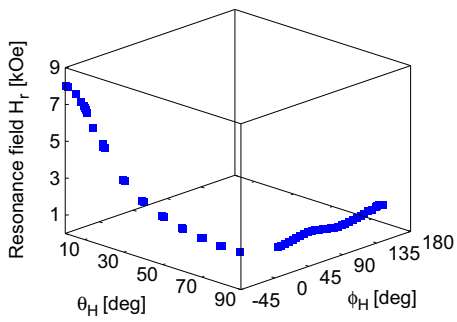

FIG. 2. Resonance field [6] H_r of the uniform SWR mode as a function of the magnetic field orientation for the out-of-plane configuration (plane H_r-ϑ_H) and for the in-plane configuration (plane H_r-φ_H).

Expressing free energy in terms of *fictitious* fields one obtains

$$f(\vartheta_H, \varphi_H, \vartheta, \varphi) = \frac{F}{M} = H_Z + H_D + H_C + H_U, \tag{2}$$

M stands here for the value of homogeneous magnetization. Dependence of fictitious anisotropy fields in Eq. (2) on the direction in space is expressed by unit vectors along the applied magnetic field **H** and along the magnetization of the sample **M**. Their spatial orientation is determined by angles ϑ_H, φ_H and ϑ, φ with respect to the [001] and [100] axes, see Fig. 1. The unit vectors are given by

$$\frac{\mathbf{H}}{H} = \left[n_x^H, n_y^H, n_z^H\right] = [\cos\varphi_H \sin\vartheta_H, \sin\varphi_H \sin\vartheta_H, \cos\vartheta_H], \tag{3a}$$

$$\frac{\mathbf{M}}{M} = [n_x, n_y, n_z] = [\cos\varphi \sin\vartheta, \sin\varphi \sin\vartheta, \cos\vartheta]. \tag{3b}$$

Zeeman field is given by

$$H_Z(\vartheta_H, \varphi_H, \vartheta, \varphi) = -H\left(n_x n_x^H + n_y n_y^H + n_z n_z^H\right). \tag{4}$$

Demagnetization field of a thin film may be approximated by the expression describing demagnetization field of an infinite plane:

$$H_D(\vartheta) = 2\pi M n_z^2. \tag{5}$$

The field $H_C(\vartheta, \varphi)$ should be invariant under the cubic symmetry transformations. It follows that it is possible to expand it into basis functions with the same symmetry. Typically, this expansion is limited to some low-order terms of systematically decreasing basis functions. The way of constructing such basis functions is presented, e.g., in Ref. [7]: they are chosen from all terms of the expansion of the identity $(n_x^2 + n_y^2 + n_z^2)^n = 1$ $(n = 2, 3...)$, which are invariant under permutation of the indices x, y, and z. Expansion up to $n = 7$ is used in what follows:

$$\begin{aligned} H_C(\vartheta, \varphi) = {} & H_{c1}\left(n_x^2 n_y^2 + n_y^2 n_z^2 + n_z^2 n_x^2\right) + H_{c2}\left(n_x^2 n_y^2 n_z^2\right) \\ & + H_{c3}\left(n_x^4 n_y^4 + n_y^4 n_z^4 + n_z^4 n_x^4\right) \\ & + H_{c4}\left(n_x^4 n_y^4 n_z^2 + n_x^4 n_y^2 n_z^4 + n_x^2 n_y^4 n_z^4\right) \\ & + H_{c5}\left(n_x^4 n_y^4 n_z^4\right) \\ & + H_{c6}\left(n_x^6 n_y^6 n_z^2 + n_x^6 n_y^2 n_z^6 + n_x^2 n_y^6 n_z^6\right). \end{aligned} \tag{6}$$

All terms included in the expansion of cubic field $H_C(\vartheta, \varphi)$ are shown in Figs. 3(a)–3(f). Let us emphasize that every next term is smaller than the previous one—the expansion Eq. (6) is convergent. Let us note, however, that the set of six basis functions used in the expansion given by Eq. (6) is neither orthogonal nor complete. Consequently, the expansion may not be unique [8]. Nevertheless, it is widely used, at least in the cases of analyzing systems with lower order magnetocrystalline anisotropies. One can also expand the cubic magnetocrystalline field $H_C(\vartheta, \varphi)$ into other basis functions, such as, e.g., spherical harmonics, remembering, however, to use only those with the appropriate symmetry [9].

It is recognized [4,7] that uniaxial anisotropy field $H_U(\vartheta, \varphi)$ in (Ga,Mn)As consist of two terms $H_{1[001]} n_z^2$ and $H_{[110]}(n_y - n_x)^2$ representing uniaxial anisotropy along z axis

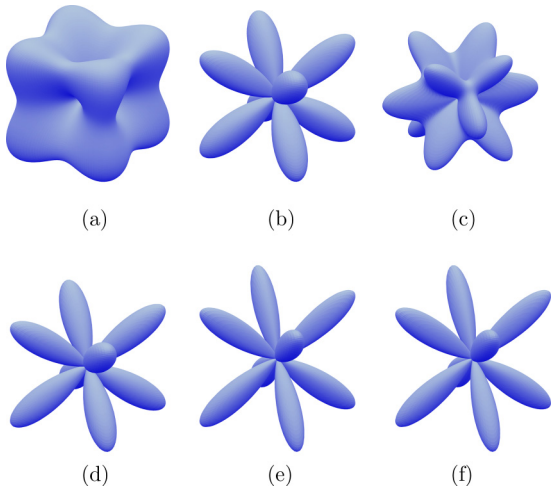

FIG. 3. The basis functions up to sixth-order (a)–(f) used in the expansion Eq. (6) of the cubic magnetocrystalline field. Although each next function of a higher order is, for given ϑ, φ, smaller than the preceding one, they are shown here as being comparable in size.

and uniaxial anisotropy along [110] axis, respectively. We add, however, two additional terms of fourth and sixth order:

$$H_U(\vartheta,\varphi) = -\tfrac{1}{2}H_{1[001]}n_z^2 - \tfrac{1}{2}H_{2[001]}n_z^4 - \tfrac{1}{2}H_{3[001]}n_z^6 - \tfrac{1}{2}H_{[110]}(n_y - n_x)^2. \quad (7)$$

Note that two terms with $\cos^2\vartheta_H$ are present in expansion given by Eq. (2): $2\pi M$ and $-\frac{1}{2}H_{1[001]}$. Usually, they are grouped together and referred to as effective anisotropy field: $H^{\text{eff}}_{[001]} = 2\pi M - \frac{1}{2}H_{1[001]}$. Four terms entering the expansion of uniaxial field $H_U(\vartheta,\varphi)$ are shown in Fig. 4.

The right side of Eq. (2) depends on 15 variables: $H_r, \vartheta_H, \varphi_H, \vartheta, \varphi, H_{c1}, ..., H_{c6}, H^{\text{eff}}_{[001]}, H_{2[001]}, H_{3[001]}, H_{[110]}$. The first three will be considered as independent variables that are measured in the experiment and are shown in Fig. 2. The pairs of angles (ϑ_H, φ_H) and (ϑ, φ) are not independent. The angles determining the equilibrium orientation of **M**, ϑ, and φ, should minimize free energy. For the set of fixed parameters $H_r, \vartheta_H, \varphi_H, H_{c1}, ..., H_{c6}, H^{\text{eff}}_{[001]}, H_{2[001]}, H_{3[001]}, H_{[110]}$, one finds them from the equilibrium condition:

$$\frac{\partial f}{\partial \vartheta} = 0, \quad \frac{\partial f}{\partial \varphi} = 0. \quad (8)$$

Thus the right-hand side of Eq. (2) really depends on ten fictitious anisotropy fields $H_{c1}, ..., H_{c6}, H^{\text{eff}}_{[001]}, ..., H_{3[001]}, H_{[110]}$, which we collectively denote by the vector

$$\mathbf{h} \equiv \left(H_{c1}, ..., H_{c6}, H^{\text{eff}}_{[001]}, H_{2[001]}, H_{3[001]}, H_{[110]}\right). \quad (9)$$

The questions should then be asked: How to find anisotropy fields and how many of them are necessary to reproduce the experimental dependence $H_r(\vartheta_H, \varphi_H)$ well? These questions are answered in the next section.

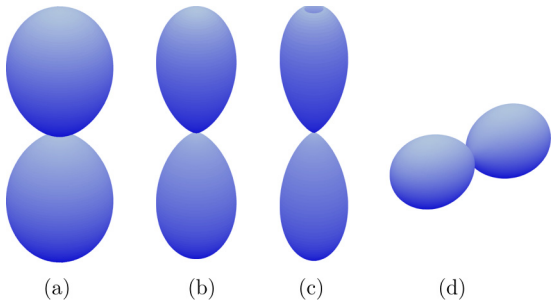

FIG. 4. Terms representing contributions to uniaxial magnetocrystalline anisotropy of (Ga,Mn)As thin film in a spherical coordinate system. Uniaxial anisotropy along z axis first to third order: n_z^2 (a), n_z^4 (b), n_z^6 (c). Uniaxial anisotropy along [110] axis $(n_y - n_x)^2$ (d).

TABLE I. Models of cubic magnetocrystalline anisotropy in (Ga,Mn)As for which cross-validation was carried out. In the second column, the terms are given included in the expansion of the free energy Eq. (6) for models C1–C6. Uniaxial anisotropy for C1–C6 models does not change—only fields $H^{\text{eff}}_{[001]}$ and $H_{[110]}$ are present.

Model	Cubic anisotropy	Uniaxial anisotropy
C1	H_{c1}	$H^{\text{eff}}_{[001]}, H_{[110]}$
C2	H_{c1}, H_{c2}	$H^{\text{eff}}_{[001]}, H_{[110]}$
C3	$H_{c1} - H_{c3}$	$H^{\text{eff}}_{[001]}, H_{[110]}$
C4	$H_{c1} - H_{c4}$	$H^{\text{eff}}_{[001]}, H_{[110]}$
C5	$H_{c1} - H_{c5}$	$H^{\text{eff}}_{[001]}, H_{[110]}$
C6	$H_{c1} - H_{c6}$	$H^{\text{eff}}_{[001]}, H_{[110]}$

III. WHICH ANISOTROPY FIELDS ARE IMPORTANT FOR (Ga, Mn)As?

The resonance condition (in the case of uniform magnetization) is given by [10,11]

$$\left(\frac{\omega}{\gamma}\right)^2 = \frac{1}{\sin^2\vartheta}\left(f_{\vartheta\vartheta}f_{\phi\phi} - f_{\vartheta\phi}^2\right), \quad (10)$$

where $f_{\vartheta\phi} = \frac{\partial f}{\partial \vartheta}\frac{\partial f}{\partial \varphi}$, $\gamma = \frac{g\mu_B}{\hbar}$ with g being the spectroscopic splitting factor, μ_B the Bohr magneton, and $\hbar$ the Planck constant. The 9.46 GHz spectrometer was used in the considered experiment [6], thus Eq. (10) reads

$$45.6834 = \frac{g^2}{\sin^2\vartheta}\left(f_{\vartheta\vartheta}f_{\phi\phi} - f_{\vartheta\phi}^2\right), \quad [\text{kOe}^2]. \quad (11)$$

TABLE II. Models of uniaxial magnetocrystalline anisotropy in (Ga,Mn)As for which cross-validation was carried out. In the second column, the terms are given included in the expansion of the free energy Eq. (4) for models U1–U3. Cubic anisotropy for U1–U3 models does not change—only fields $H_{c1} - H_{c4}$ are present.

Model	Uniaxial anisotropy	Cubic anisotropy
U1	$H^{\text{eff}}_{[001]}, H_{[110]}$	$H_{c1} - H_{c4}$
U2	$H^{\text{eff}}_{[001]}, H_{2[001]}, H_{[110]}$	$H_{c1} - H_{c4}$
U3	$H^{\text{eff}}_{[001]}, H_{2[001]}, H_{3[001]}H_{[110]}$	$H_{c1} - H_{c4}$

TABLE III. Anisotropy fields [Oe] in bulk (Ga,Mn)As related to cubic and uniaxial symmetry and values of g factor calculated for models C1–C6, according to the procedure described in the text. In the last two columns, error functions $\langle E^{N-1}_{\mathrm{RMS}}\rangle$ and $\langle E^{1}_{\mathrm{RMS}}\rangle$ are shown.

Model	H_{c1}	H_{c2}	H_{c3}	H_{c4}	H_{c5}	H_{c6}	$H^{\mathrm{eff}}_{[001]}$	$H_{[110]}$	g	$\langle E^{N-1}_{\mathrm{RMS}}\rangle$	$\langle E^{1}_{\mathrm{RMS}}\rangle$
C1	91.81						4765	65.53	1.978	0.95	0.69
C2	92.21	−87.94					4774	70.72	1.979	0.88	0.68
C3	77.06	−4.241	57.00				4776	61.70	1.982	0.75	0.61
C4	78.07	−534.1	43.93	1405			4811	66.29	1.985	0.59	0.50
C5	79.57	−583.4	41.68	1790	2080		4814	64.50	1.984	0.58	0.48
C6	78.78	−419.0	41.82	436.1	2841	2700	4809	63.81	1.984	0.57	0.51
Liu *et al.* [6]	197[a]						4588	77	1.98		

[a]Note that definition of cubic anisotropy in Ref. [6] is slightly different. It takes into account tetragonal distortion in (GaMn)As thin films. The value of cubic anisotropy field calculated from this definition should be approximately equal to $2H_{c1}$.

At resonance, Eq. (11) should be met for any given direction of $\mathbf{H}_r(\vartheta_H, \varphi_H)$, i.e., in the case under consideration, for all points shown in Fig. 2. Let us treat g and components of the vector $\mathbf{h}$ as not known parameters and denote the right-hand side of the Eq. (11) calculated at ith experimental point by R_i,

$$R_i(g,\mathbf{h}) = \frac{g^2}{\sin^2\vartheta}\left(f^i_{\vartheta\vartheta}f^i_{\phi\phi} - \left(f^i_{\vartheta\phi}\right)^2\right). \tag{12}$$

Note that free energy derivatives (e.g., $f^i_{\vartheta\vartheta}$) are calculated at ith the experimental point for given values $H_r, \vartheta_H, \varphi_H$.

One should find such values of unknown coefficients $g, \mathbf{h}$ that the Eq. (11) is met as accurately as possible for each experimental point. So the following error function, being the positive square root of the sum of squares of residuals,

$$E^N_{\mathrm{RMS}}(g,\mathbf{h}) = \sqrt{\frac{1}{N}\sum_i \left(R_i(g,\mathbf{h}) - 45.6834\right)^2}, \tag{13}$$

should be minimized in 11-dimensional parameter space $(g, \mathbf{h})$. The sum in Eq. (13) runs over all N experimental points shown in Fig. 2. This least-squares approach to finding the unknown parameters represents a specific case of *maximum likelihood* approach [12,13]. Actual values of the spectroscopic splitting factor g and magnetocrysralline anisotropy fields are those for which Eq. (13) has a minimum close to zero.

We have included ten magnetocrysralline anisotropy fields into the formula for free energy. Now we will check which ones are really essential to describe the experimental results well using a simple *cross-validation* scheme [12]. For this purpose, anisotropy models are defined in Tables I and II. For example, in the model C3 (third row of Table I) the cubic anisotropy is expanded up to third order, the uniaxial anisotropy along z axis up to first order, the uniaxial anisotropy along [110] axis up to first order and similarly for other models.

The cross-validation, within *leave-one-out technique*, runs as follows: We divide the N (=55) element set of experimental data into two subsets: the training one and the test one. The first one contains $N-1$ elements, the second one—one element. One can do it in N possible ways. Subsequently, the N subsets obtained in this way are used to train, i.e., to determine the values of the unknown parameters $(g, \mathbf{h})$ by minimizing the error function $E^{N-1}_{\mathrm{RMS}}(g, \mathbf{h})$, defined in Eq. (13) for each model under consideration. Simultaneously, the error function $E^1_{\mathrm{RMS}}(g, \mathbf{h})$ is calculated for one left test point for each model. Note that its value informs us how well we are doing in predicting the values of anisotropy fields for a particular model. After N minimizations, one examines how averages $\langle E^{N-1}_{\mathrm{RMS}}\rangle$ and $\langle E^1_{\mathrm{RMS}}\rangle$ depend on the model, i.e., on the order of expansion in Eqs. (6) or (7). We use the following criterion to assess the quality of the model: the model describes magnetocrystalline anisotropy well if taking into account higher order terms in the expansions given by Eqs. (6) and (7) does not improve its predictive ability given by the average $\langle E^1_{\mathrm{RMS}}\rangle$.

The procedure described above allowed us to find the average values of anisotropy fields, g factor, and error functions $\langle E^{N-1}_{\mathrm{RMS}}\rangle$ and $\langle E^1_{\mathrm{RMS}}\rangle$ for each model after N minimizations for the sample in the experiment under consideration. They are collected in Tables III and IV. The predictive ability, measured by the error function $\langle E^1_{\mathrm{RMS}}\rangle$, for all models defined in Tables I and II is shown in Fig. 5. $\langle E^1_{\mathrm{RMS}}\rangle$ decreases for C1–C4 models and remains roughly constant for the C4–C6 models. It means that higher order terms used in free energy expansion given by Eq. (2) for C5 and C6 models do not improve their ability to predict cubic magnetocrystalline anisotropy on the basis of experimental data from Fig. 2. Similarly, we see that

TABLE IV. Anisotropy fields [Oe] in bulk (Ga,Mn)As related to cubic and uniaxial symmetry and values of g factor calculated for models U1–U3, according to the procedure described in the text. In the last two columns, error functions $\langle E^{N-1}_{\mathrm{RMS}}\rangle$ and $\langle E^{1}_{\mathrm{RMS}}\rangle$ are shown.

Model	$H^{\mathrm{eff}}_{[001]}$	$H_{2[001]}$	$H_{3[001]}$	$H_{[110]}$	H_{c1}	H_{c2}	H_{c3}	H_{c4}	g	$\langle E^{N-1}_{\mathrm{RMS}}\rangle$	$\langle E^{1}_{\mathrm{RMS}}\rangle$
U1	4811			66.28	78.07	−534.1	43.93	1405	1.985	0.59	0.50
U2	4779	21.83		66.08	80.12	−449.3	40.76	1222	1.987	0.59	0.51
U3	4778	21.99	6310	66.13	80.15	−449.3	40.59	1221	1.987	0.59	0.50

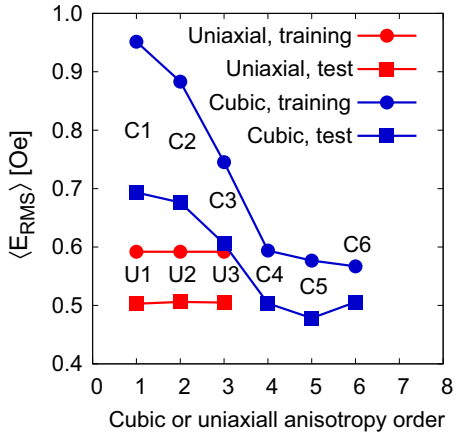

FIG. 5. The values of error functions $\langle E^{N-1}_{\mathrm{RMS}}\rangle$ and $\langle E^{1}_{\mathrm{RMS}}\rangle$ defined in Eq. (12) for all models defined in Tables I and II. The values error functions were calculated for the corresponding field values taken from Tables III and IV.

taking into account higher order terms in uniaxial anisotropy expansion for models U2 and U3 does not improve their predictive ability. It follows that the correct description of magnetocrystalline anisotropy in (GaMn)As requires that the free energy expansion should include terms describing cubic anisotropy up to fourth order and that is enough to take into account uniaxial anisotropies up to first order.

One can also see the result of minimization in Fig. 6 in the form of a collapse: for the real minimum of error function at $g^*, \mathbf{h}^*$ its values $R_i(g^*, \mathbf{h}^*)$ for all experimental points fall onto a line 45.6834. By comparing the scattering of points for C1 model, Fig. 6(a), and C4 model, Fig. 6(b), we note the important thing: the addition of the higher orders of cubic anisotropy fields improves fitting not only for *in-plane* experimental points but also for *out-of-plane* experimental points. This is due to the occurrence of partial mixed derivatives of the free energy in the determinant from Hessian (representing a local curvature of free energy in ϑ_H, φ_H space)

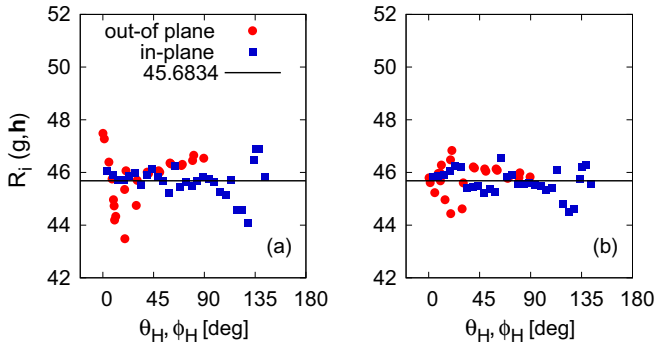

FIG. 6. The values of function $R_i(g, \mathbf{h})$ defined in Eq. (12) for model C1(a) and for model C4 (b) for all experimental points from Fig. 2. Squares—in-plane geometry: $\vartheta_H = 90^\circ$, φ_H changes; circles—out-of-plane geometry: ϑ_H changes, $\varphi_H = -45^\circ$. The values of $R_i(g, \mathbf{h})$ were calculated for the corresponding field values taken from Table III.

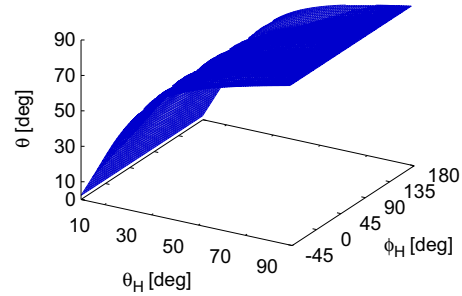

FIG. 7. Equilibrium magnetization angle ϑ versus the external field angles ϑ_H, φ_H determined from the condition Eq. (8) for the (Ga,Mn)As thin film studied in Ref. [6].

in Smit-Beljers Eq. (10) which we solve numerically[1] for all experimental points simultaneously treating them on equal footing. Therefore, to get as accurate as possible anisotropy field values it is important to measure resonance fields in different geometries.

Fulfilling condition Eq. (8) while solving Eq. (13) leads to finding dependences $\vartheta(\vartheta_H, \varphi_H)$ and $\varphi(\vartheta_H, \varphi_H)$ for all models from Tables III and IV. They are shown for C4 model in Figs. 7 and 8. Function $\vartheta(\vartheta_H, \varphi_H)$ for a given φ_H—it always is a concave function. For angle $\phi_H = 45^\circ$ and 135°, we see a ripple, which is the result of the presence of cubic symmetry. Note also that function $\varphi(\vartheta_H, \varphi_H)$ for a given ϑ_H is for all ϑ_H a linear function $\varphi \propto \varphi_H$ (does not depend on ϑ_H).

Let us summarize this section by stating that for the correct description of magnetocrystalline anisotropy in (Ga,Mn)As, the free-energy expansion should include terms describing cubic anisotropy up to fourth order and that is enough to take into account uniaxial anisotropies up to first order.

IV. BACK TO THE EXPERIMENT: WHAT IS THE EFFECT OF INCORPORATING ANISOTROPY FIELDS OF HIGHER ORDERS?

Let us now examine the dependence of the resonance field H_r on ϑ_H and φ_H. The problem can be stated in the following way: Given the values of H_r on the boundary of the box presented in Fig. 2, determine the resonance field

[1]We use Python packages SCIPY.OPTIMIZE and NUMDIFFTOOLS.

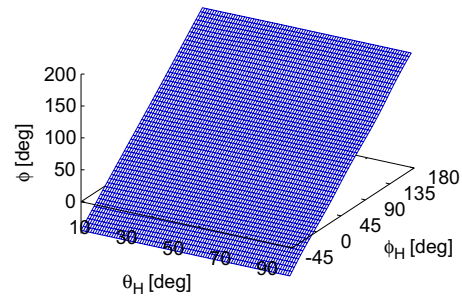

FIG. 8. Equilibrium magnetization angle φ versus the external field angles ϑ_H, φ_H determined from the condition Eq. (8) for the (Ga,Mn)As thin film studied in Ref. [6].

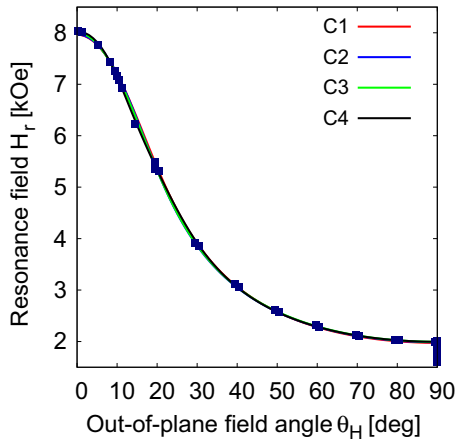

FIG. 9. Comparison of the H_r-values calculated numerically from Eq. (10) with experimental data (full squares) for out-of-plane geometry for C1–C4 models. The resonance field for in-plane geometry measurement is visible as a small rectangle on the vertical axis for $\vartheta_H = 90^\circ$.

inside the box. One finds a solution in two stages. First, one determines the anisotropy fields, for which Eq. (11) is satisfied on the boundary of the box. This stage has been described in Sec. III. Second, to get the resonance field for each ϑ_H and each φ_H, one should solve Eq. (11) numerically for the anisotropy fields determined in the first stage (collected in Table III) with condition Eq. (8) met for each tentative point obtained during the numerical solving procedure. In Figs. 9 and 10, one can see dependencies $H_r(\vartheta_H, -45^\circ)$, i.e, for out-of-plane geometry and $H_r(90^\circ, \varphi_H)$ for in-plane geometry, respectively. Uniaxial anisotropy is the most visible for out-of-plane geometry (Fig. 9) and although the use of higher order cubic terms does improve the agreement of the calculated H_r-values with the experimental data, this improvement is not particularly visible in the scale of Fig. 9 because the cubic anisotropy is much smaller than the uniaxial one. The improvement, however, can be seen for in-plane geometry: the use of higher order terms in of cubic anisotropy expansion

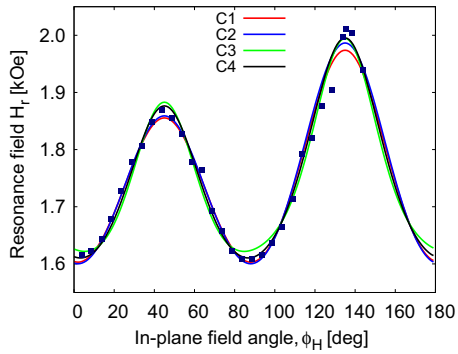

FIG. 10. Comparison of the H_r-values calculated numerically from Eq. (10) with experimental data (full squares) for in-plane geometry for C1–C4 models. Taking into account higher order terms of cubic anisotropy, one improves the agreement of calculated H_r-values with experimental data.

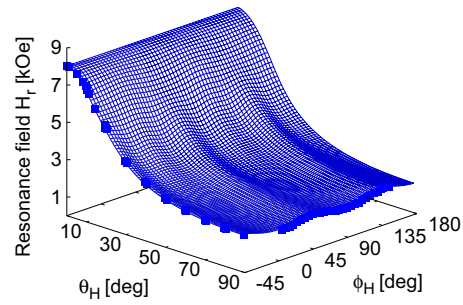

FIG. 11. Spatial angular dependence of resonance field $H_r(\vartheta_H, \varphi_H)$ resulting from our theory. Experimental data (squares) in the plane (H_r, ϑ_H) correspond to out-of-plane geometry while those in the (H_r, φ_H) plane to in-plane geometry. The surface in the figure is the numerical solution of Eq. (11) with condition Eq. (8).

given by Eq. (6) becomes necessary to describe dependence $H_r(90^\circ, \varphi_H)$ more precisely.

The spatial dependence of the resonance field on angles ϑ_H and φ_H is shown in Fig. 11. For small angles ϑ_H, we see the resonance field whose source is mainly uniaxial [001] anisotropy (with twofold symmetry), whereas for angles $\vartheta_H \approx 90^\circ$ the resonance field with fourfold symmetry becomes more noticeable. It is the result of cubic anisotropy, although $H_r(90^\circ, 45^\circ) < H_r(90^\circ, 135^\circ)$ due to small uniaxial [110] anisotropy, see also Fig. 10.

The spatial dependence of the cubic anisotropy field is shown in Fig. 12. We see that really the magnetic field determines hard/easy directions, not hard/easy axes: The largest cubic anisotropy field is for $\vartheta_H = 23.7^\circ$ and $\varphi_H = 45^\circ$ whereas the position of hard axis direction is given by $\vartheta_H = 54.7^\circ$ and $\varphi_H = 45^\circ$.

The values of fictitious anisotropy fields are important in that they allow us to reproduce the spatial dependence of the energy of the sample in a magnetic field due to magnetocrystalline anisotropy and to find easy and hard axes. To find this spatial dependence, one needs to know the saturation magnetization. Then the magnetic anisotropy constants can be easily expressed by corresponding anisotropy fields, see, e.g., very clearly written Ref. [14]. We have found the saturation magnetization[2] of the considered sample: it amounts $M_s = 30.5$ emu/cm^3, which is a typical value for (Ga,Mn)As containing a few percents of Mn atoms.

[2]Details of this calculation will be published in a separate paper.

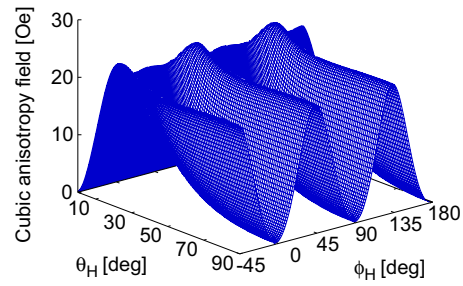

FIG. 12. Cubic anisotropy field for C4 model versus ϑ_H and φ_H.

TABLE V. Cubic anisotropy fields (H_c) in Gaussian units [Oe] and SI units [kA/m] and cubic anisotropy constants (K_c) in [erg/cm^3] and [J/m^3] for bulk (Ga,Mn)As calculated for models C1 and C4.

Model C1	H_{c1}	H_{c2}	H_{c3}	H_{c4}	K_{c1}	K_{c2}	K_{c3}	K_{c4}
Gaussian	91.81 ± 0.55				2800 ± 17			
SI	7.306 ± 0.044				280.0 ± 1.7			
Model C4								
Gaussian	78.07 ± 0.40	-534 ± 28	43.9 ± 1.2	1410 ± 70	2381 ± 13	-16280 ± 860	1330 ± 37	42900 ± 220
SI	6.213 ± 0.032	-42.5 ± 2.3	3.493 ± 0.096	112.2 ± 5.6	238.1 ± 1.3	-1628 ± 86	133.0 ± 3.7	4290 ± 22

Returning to the Eq. (6) and multiplying it by M_s, one obtains the spatial distribution of energy $F_C(\vartheta, \varphi)$ stored in bulk (Ga,Mn)As and related to its cubic magnetocrystalline anisotropy for the C4 model

$$\begin{aligned} F_C(\vartheta,\varphi) &= M_s H_{c1}\left(n_x^2 n_y^2 + n_y^2 n_z^2 + n_z^2 n_x^2\right) + M_s H_{c2}\left(n_x^2 n_y^2 n_z^2\right) \\ &\quad + M_s H_{c3}\left(n_x^4 n_y^4 + n_y^4 n_z^4 + n_z^4 n_x^4\right) \\ &\quad + M_s H_{c4}\left(n_x^4 n_y^4 n_z^2 + n_x^4 n_y^2 n_z^4 + n_x^2 n_y^4 n_z^4\right) \\ &\equiv K_{c1}\left(n_x^2 n_y^2 + n_y^2 n_z^2 + n_z^2 n_x^2\right) + K_{c2}\left(n_x^2 n_y^2 n_z^2\right) \\ &\quad + K_{c3}\left(n_x^4 n_y^4 + n_y^4 n_z^4 + n_z^4 n_x^4\right) \\ &\quad + K_{c4}\left(n_x^4 n_y^4 n_z^2 + n_x^4 n_y^2 n_z^4 + n_x^2 n_y^4 n_z^4\right), \end{aligned} \tag{14}$$

and similarly for the C1 model. K_{c1}–K_{c4} stand in Eq. (14) for cubic anisotropy constants. Taking the numerical values of anisotropy fields H_{c1}–H_{c4} from Table III, one obtains the numerical values of anisitropy constants for C1 and C4 models—they are collected in Table V. Let us note that the values of first-order cubic anisotropy for (Ga,Mn)As are several dozens to several hundred times smaller than the corresponding values for such ferromagnets as Ni or Fe. Perhaps this is why anisotropies of higher orders become visible in resonance experiments only for weak ferromagnets.

To assess the accuracy of the present method, we used the bootstrap method to evaluate errors for C1 and C4 models. To do this, we assumed that the error probability distribution of experimental results was normal and, consequently, the errors of a solution of Smit-Beljers equation also had a normal distribution. Then we could determine the approximated errors of obtained anisotropy constants. They are listed in Table V.

Finally, let us show how taking into account the higher orders of anisotropy fields changes the cubic anisotropy energy surface. It might seem that correction will be of little importance. However, this is not the case: the Smit-Beljers Eq. (10) describing the curvature of the energy surface is nonlinear with respect to the second derivatives. This leads to significant corrections in energy values. Figure 13 shows the spatial dependence of energy from cubic anisotropy on the same scale for models C1 and C4. Axes [100], [010], and [001] are easy axes with respect to cubic anisotropy, and axis [111] is a hard one. For example, for hard axis we have $F_{C1}([111]) = 933 \pm 6$, $F_{C4}([111]) = 769 \pm 4$ [erg/cm^3]. The C1 model thus overestimates the anisotropy energy along the hard axis by about 20%. Figure 14 shows the spatial dependence of energy difference between C1 and C4 models.

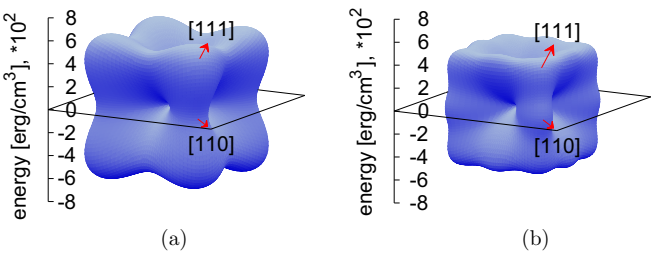

FIG. 13. Spatial dependence of the cubic magnetocrystalline energy in spherical coordinate system for C1 (a) and C4 (b) models.

V. SUMMARY AND OUTLOOK

The paper presents how to determine bulk magnetocrystalline anisotropy in (Ga,Mn)As thin film by numerical solution of the Smit-Beljers equation for all data collected in one FMR experiment, i.e., for different spatial orientations of the magnetic field with respect to the sample, on equal footing. To avoid essential drawbacks of fitting procedures (lack of information which fitted constants are relevant and the possibility of overfitting) by finding anisotropy constants, we cross-validated the numerical solutions of Smit-Beljers equation for six models (C1–C6). The results of this cross-validation, i.e., the values of the function $\langle E^1_{\mathrm{RMS}} \rangle$ displaying predictive ability for models C1–C6 point that it is necessary to expand bulk cubic anisotropy up to the fourth order to reproduce spatial dependence of the resonance field correctly—that is, increasing the order of expansion of anisotropy does not change the predictive ability of the model under consideration. Such cubic anisotropy (up to fourth order) is visible in the resonant experiment. It means that the models of first-order cubic anisotropy applied so far to (Ga,Mn)As overestimated

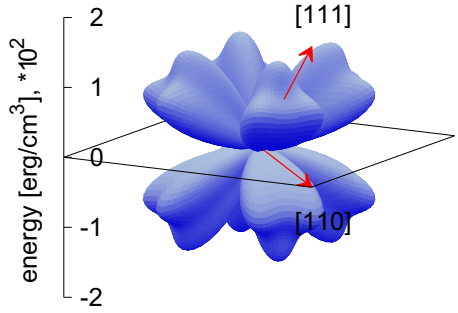

FIG. 14. Spatial dependence of the difference of cubic magnetocrystalline energy between C1 and C4 models in spherical coordinate system.

the value of this anisotropy. Let us stress that this description of the bulk anisotropy is consistent with the presented earlier description [5] of the surface anisotropy (both descriptions require higher order expansion of cubic anisotropy). We also have shown that FMR data allow one to find the spectroscopic splitting factor with high accuracy. We intend to confirm the usefulness of this new approach by applying it to other available resonance experiments in the near future.

ACKNOWLEDGMENTS

The authors would like to thank Marcin Tomczak for stimulating discussions. This study is part of a project financed by Narodowe Centrum Nauki (National Science Centre of Poland), Grant No. DEC-2013/08/M/ST3/00967. Numerical calculations were performed at Poznań Supercomputing and Networking Center under Grant No. 284.

[1] U. Welp, V. K. Vlasko-Vlasov, X. Liu, J. K. Furdyna, and T. Wojtowicz, Phys. Rev. Lett. **90**, 167206 (2003).
[2] X. Liu, Y. Sasaki, and J. K. Furdyna, Phys. Rev. B **67**, 205204 (2003).
[3] G. Nieuwenhuys, T. Prokscha, A. Suter, E. Morenzoni, D. Chiba, Y. Nishitani, T. Tanikawa, F. Matsukura, H. Ohno, J. Ohe, S. Maekawa, and Y. J. Uemura, Nat. Mater. **9**, 299 (2010).
[4] X. Liu and J. K. Furdyna, J. Phys.: Condens. Matter **18**, R245 (2006).
[5] H. Puszkarski and P. Tomczak, Surf. Sci. Rep. **72**, 351 (2017).
[6] X. Liu, Y. Y. Zhou, and J. K. Furdyna, Phys. Rev. B **75**, 195220 (2007).
[7] J. Zemen, J. Kučera, K. Olejník, and T. Jungwirth, Phys. Rev. B **80**, 155203 (2009).
[8] E. Callen and H. Callen, J. Phys. Chem. Solids **16**, 310 (1960).
[9] H. Puszkarski, Prog. Surf. Sci. **9**, 191 (1979).
[10] J. Smit and H. G. Beljers, Philips Res. Rep. **10**, 113 (1955).
[11] L. Baselgia, M. Warden, F. Waldner, S. L. Hutton, J. E. Drumheller, Y. Q. He, P. E. Wigen, and M. Maryško, Phys. Rev. B **38**, 2237 (1988).
[12] C. M. Bishop, *Pattern Recognition and Machine Learning* (Springer, New York, 2006).
[13] P. Mehta, M. Bukov, C.-H. Wang, A. G. R. Day, C. Richardson, C. K. Fisher, and D. J. Schwab, arXiv:1803.08823v1.
[14] M. W. Gutowski, arXiv:1312.7130v1.